International Journal of Numerical Methods for Heat & Fluid Flow

# Impact of fluid–structure interaction on unsteady flow within wavy-heated wall cavity

Habibis Saleh
*School of Mathematical Sciences, Universiti Kebangsaan Malaysia, Bangi, Malaysia, and Mathematics Education Department, Universitas Islam Negeri Sultan Syarif Kasim Riau, Pekanbaru, Indonesia*

Ammar I. Alsabery
*Refrigeration and Air conditioning Technical Engineering Department, College of Technical Engineering, The Islamic University, Najaf, Iraq*

Mikhail Sheremet
*Laboratory on Convective Heat and Mass Transfer, Tomsk State University, Tomsk, Russia*

Mohammed Glalmbaz
*Department of Mathematical Sciences, Saveetha School of Engineering, SIMATS, Chennai, India, and Laboratory on Convective Heat and Mass Transfer, Tomsk State University, Tomsk, Russia, and*

Ishak Hashim
*Department of Mathematical Sciences, Faculty of Science and Technology, Universiti Kebangsaan Malaysia, Bangi, Malaysia, and Nonlinear Dynamics Research Center (NDRC), Ajman University, Ajman, United Arab Emirates*

Received 20 January 2025
Revised 2 March 2025
4 March 2025
Accepted 4 March 2025

**Abstract**

**Purpose** – This study aims to explore impact of fluid−structure interaction (FSI) analysis on the unsteady convection heat transfer in wavy-heated wall cavity.

**Design/methodology/approach** – The arbitrary Lagrangian Eulerian approach within an unstructured mesh and the finite-element method are used to determine the governing partial differential equation.

**Findings** – A number of factors influence the thermal design and formation of circulation flow, including Rayleigh number, wall flexibility, amplitude and undulations. Changes in the undulation number and flexible wall can have a notable impact, especially in the core regions and near the hot wall. One and two undulation at large amplitude and high Rayleigh number cases penetrated toward improved heat transfer and the appearance of flexible surfaces.

**Originality/value** – This study presents a novel computational investigation of FSI effects on unsteady flow and heat transfer dynamics in wavy-walled cavities, addressing the gap in prior rigid-boundary assumptions by incorporating dynamic wall deformation. By coupling advanced numerical modeling of transient fluid dynamics and structural elasticity, the work uniquely examines how time-dependent interactions between a flexible right wall

The authors thank the respected reviewers for their constructive comments which clearly enhanced the quality of the manuscript. This research of Mikhail Sheremet and Mohammad Ghalambaz was supported by the Tomsk State University Development Programme (Priority-2030).

International Journal of Numerical Methods for Heat & Fluid Flow

0961-5539
DOI 10.1108/HFF-01-2025-0045

and natural convection alter thermal performance, flow instabilities and momentum transfer in wavy geometries. The analysis reveals how structural deformation modulates heat transfer efficiency under unsteady conditions.

**Keywords** FEM (finite-element method), FSI (fluid structure interaction), Elastic wall, Transient convection, Wavy wall

**Paper type** Research paper

## 1. Introduction

Free convection process found in wavy enclosures is of relevance to many engineer considering its broad applications, for example those found in micro-electric devices, heat exchangers, solar energy collectors and nuclear reactors. The alteration of surface waviness and its types is regarded as a regulating criterion for evaluating the features of heat and flow fields. A considerable body of evidence demonstrates that the thermal transfer coefficient is markedly elevated because of the induced turbulent mixing and an expanded heat transfer area relative to a flat surface. Alternative configurations in the interface of concurrent or countercurrent two-phase flow.

Wavy geometries enhance heat transfer across mixed, natural and forced convection regimes. In mixed convection with $Fe_3O_4$/multi-walled carbon nanotubes-water nanofluids, higher $Da$ ($10^{-5}$–$10^{-2}$) and lower $Ha$ (0–10) amplify heat transfer in porous cubic cavities via reduced magnetic damping (Jiang *et al.*, 2023). Natural convection of nano-encapsulated phase change material in wavy enclosures shows $Ra = 10^6$ quadruples local $Nu$ vs $Ra = 10^3$, while $Ha$ = 100 suppresses $Nu$ by 38% (Alazzam *et al.*, 2023). Trapezoidal cavities with nanofluids ($\phi = 0.06$) reveal higher temperature gradients boost $Nu$, but $Ha = 25 - 100$ aligns flow, damping turbulence (Shandar *et al.*, 2025). Square cavities with corrugated rods highlight sensitivity to $Ra$, $Ha$ and undulations for electronics/nuclear applications (Nadeem *et al.*, 2023). Conjugate analysis in wavy minichannels ($\alpha = 0.2,\ 5 \leq Re \leq 15$) yields higher $Nu$ and PF, vital for solar/heating, ventilation, and air conditioning systems (Borah *et al.*, 2023).

Valuable works of Saidi *et al.* (1987) have contributed to the initial advancement of mathematical modeling for natural research within wavy enclosures. Authors presented the streamlines and isotherms of inside the wavy enclosure and stated that the total thermal transmission of the wavy surface and the moving fluid was diminished as a result of existence of the vortices. Adjlout *et al.* (2002) observed that the heated undulating surface changed flow within the hollow and the rate at which heat transferred. Mahmud *et al.* (2002) found that by decreasing waviness of the surface, the higher heat transfer drops or grows constantly depending on the surface waviness parameter. Das and Mahmud (Das and Mahmud, 2003) studied enclosure consists of the cavity including two wavy surfaces and double straight surfaces. The amplitude-wavelength ratio was found small effect heat transfer performance. Convective heat transfer is found by Morsi and Das (2003) to be significantly modified by the waviness effect. Mahmud and Islam (2003) reported the averaged entropy generation rate toward a variety of wave ratios. Mahmud and Fraser (2004) studied an enclosure with double horizontal straight surfaces and double vertical undulating surfaces where it follows a trigonometry profile. Sabeur-Bendehina *et al.* (2006) delineated the propensity of heat transfer rate influenced by different aspect ratios of wavy geometry. Abdelkader *et al.* (2007) demonstrated that heat transmission and flow patterns were significantly influenced by the amplitude of a heated wavy bottom surface. Hussain and Mohammed (2011) concluded that the thermal performance remains diminished by improving Rayleigh number on the left wavy sidewall, whereas thermal performance enhances with the rise of Rayleigh on the right wavy sidewall for the inclined enclosure. Hasan *et al.* (2012) found that the development of convective flows supports three platforms:

Initial platform, transitional or oscillatory platform and steady platform. Tekkalmaz (2013) studied the effects of heating the lower surface and cooling the upper surface of a cavity. Sheikholeslami *et al.* (Sheikholeslami *et al.*, 2014) examined a chamber with nanofluids to see how magnetic field effects, orientation and waviness affect heat transfer. Transient streamlines, isotherms and isoconcentrations of nanofluids are examined by Sheremet *et al.* (2016) concerning a wavy-walled enclosure under the magnetic field impact. Alsabery *et al.* (2018) and Hashim *et al.* (2018) considered an inner block the cavity filled nanoparticles and host fluid where the goal is to choose an optimal waviness configuration. Cho (2019) investigated steady convection and entropy formation within a wavy-wall lid-driven hollow containing nanofluids and magnetic fields. Recently, Salehpour *et al.* (2019) conducted a simulation for transient convection within a rectangular cavity loaded by a power-law non-Newtonian liquid for corrugation amplitudes from 0.1 to 0.5, and frequency 1–5. Different nanoparticle shape and undulation plate was found by Dogonchi *et al.* (2020) to have the significant influence in the thermal performance. Chattopadhyay *et al.* (2020) stated that the undulating wall direction influences convection.

It was seen that the majority of subjects were located in the thermal transfer region of wavy cavities with rigid surfaces. It has a thin profile, is flexible and offers a wide range of thermal characteristics as a result of the new material. A new engineered material offers a pliable surface that boasts enhanced elastic properties, remarkable thinness and diverse thermal characteristics. For instance, inelastic water manifold operations under expected radiation during solar drying use very thin membranes to protect electrical components, the membranes demonstrate significant elasticity and are influenced by the circulation of fluid (Alsabery *et al.*, 2019a). Flexible walls are frequently oscillated or shifted inside elastic domains, while solids are forced by fluids to conform at stress boundary conditions. Engel and Griebel (2006) asserted that the fluid's response to a solid's flexible deformation is contingent upon the moving boundary's position and velocity. By depicting the displacement and velocity contours of the interface, he showed how fluid dynamics exerted forces on a flexible body. Rigid and elastic wall aneurysm models exhibit significant differences in flow field configurations, as delineated by Khanafer *et al.* (2009). The convection inside a cavity with a flexible bottom surface was numerically evaluated by Al-Amiri and Khanafer (2011). Khanafer (2013) analyzed the Nusselt number, isotherms and streamlines of stiff as well as a flexible right wall. According to their findings, the intensity of heating and the elasticity of the flexible surface significantly influence the morphology of the flexible surface, hence enhancing heat transfer. Khanafer (2014) subsequently conducted a study between wavy and flexible geometries concerning bottom-heated surfaces. Wang and Davidson (2016) showed that rigid manifolds performed better than flexible manifolds due to entrainment collapse. Selimefendigil and Oztop (2016) examined a cavity with a flexible wall filled with nanofluids exhibiting volumetric generation of heat by magnetohydrodynamic mixed convection. Jamesahar *et al.* (2016) examined a flexible diagonal separator with high thermal conductivity. Raisi and Arvin (2018) investigated the upper flexible wall, resulting in improved heat transport and augmented deformations of the flexible components by increasing the Rayleigh number. Selimefendigil and Oztop (2017) studied the heat generation of localized heated triangular containers containing nanofluids that have elastic surfaces and internal heating sources (Selimefendigil *et al.*, 2017). Following that, Selimefendigil *et al.* (2019a) reached the cavity that was driven by a lid, along with elastic walls on top. A bottom wall's flexibility in a vented cavity has been explored later by Selimefendigil *et al.* (2019b) in relation to an internal L-shaped conductive obstacle. As a result of using the flexible in an inclined L-enclosure, Selimefendigil and Oztop (2019) achieved an 11% improvement in heating efficiency. Alsabery *et al.* (2019b) investigated how heat is transferred and entropy is

produced within cavities containing an elastic right surface and a rotating active cylinder. Ghalambaz *et al.* (2019) examined the heating of nonuniform temperatures within a square enclosure separated by flexible membranes. Ghalambaz *et al.* (2020) determined that a pseudoplastic material enhanced the elastic heater's thermal properties. Mehryan *et al.* (2020a) discovered that the least tension and deformation occurred in the center of the plate with elastic properties. Mehryan *et al.* (2020b) discovered that intensifying the heating enhances heat performance and wall tension. Shahabadi *et al.* (2021) demonstrated that heat transfer through a hot wall is not consistent with Young's modulus.

In an L-shaped enclosure with a flexible fin and elastic wall, sinusoidal forces applied to both components induce periodic oscillations, increasing the Nusselt number on hot walls by up to 28% at higher amplitudes and frequencies (Ahmed and Razavi, 2024). The elasticity of the wall further amplifies this effect, with lower elastic modulus values (i.e. greater flexibility) enhancing *Nu* due to larger deformations that intensify flow recirculation (Ahmed and Razavi, 2024). Similarly, in lid-driven cavities with a flexible sidewall, the combination of wall motion and flexibility boosts *Nu* by 28% compared to stationary rigid configurations, with the direction of top-wall movement (left vs right) critically influencing flow vorticity and thermal mixing (Yaseen *et al*., 2023).

The interplay between thermal and structural parameters governs these enhancements. In natural convection within L-shaped wavy enclosures featuring a flexible baffle, higher Rayleigh numbers (*Ra*) strengthen buoyancy-driven flows, while reduced elasticity modulus (E) promotes baffle deflection, creating secondary circulation zones that augment heat transfer (Alrasheedi, 2024). These circulation zones, influenced by *Ra* and *E*, disrupt thermal stratification and improve convective efficiency, particularly in systems requiring adaptive thermal management (Alrasheedi, 2024). Similarly, in 3D cavities with oscillating plates, proximity to heated walls amplifies the local heat transfer coefficient by 8% when the plate is positioned 25 mm from the right wall compared to 75 mm, as plate oscillations generate turbulence near high-temperature regions (Hashemi *et al.*, 2024). Thinner oscillating plates (0.4 mm vs 1 mm) further improve performance by 4.24%, emphasizing the role of geometric flexibility in optimizing thermal exchange (Hashemi *et al.*, 2024).

Operational parameters such as Richardson number (*Ri*) and Reynolds ratio (*Rer*) also modulate flexible-wall efficacy. In mixed convection, lower *Ri* values ($0.01 \leq Ri \leq 100$) favor inertial forces over buoyancy, enabling flexible walls to amplify shear-driven mixing, while higher *Rer* ratios ($1 \leq Rer \leq 4$) enhance inlet momentum, synergizing with wall oscillations to redistribute heat (Yaseen *et al.*, 2023). Notably, the synergy between multiple flexible components − such as fins and walls-yield cumulative enhancements, as seen in L-shaped enclosures where combined flexibility elevates *Nu* beyond the sum of individual contributions (Ahmed and Razavi, 2024).

This study presents a novel computational investigation of fluid−structure interaction (FSI) effects on unsteady flow and heat transfer dynamics in wavy-walled cavities, addressing the gap in prior rigid-boundary assumptions by incorporating dynamic wall deformation. By coupling advanced numerical modeling of transient fluid dynamics and structural elasticity, the work uniquely examines how time-dependent interactions between a flexible right wall and natural convection alter thermal performance, flow instabilities and momentum transfer in wavy geometries. The analysis reveals how structural deformation modulates heat transfer efficiency under unsteady conditions.

## 2. Mathematical formulation

Wavy wall surfaces and flexible enclosures have diverse applications, including enhancing heat exchangers by increasing surface area for better heat transfer. In thermal management

for electronics, flexible walls adapt to fluid flow, improving heat dissipation in devices like microprocessors. In addition, these systems are useful for energy harvesting, converting thermal gradients into mechanical work, thereby contributing to self-sustaining renewable energy generation systems, making them ideal for applications in solar thermal and thermoelectric technologies. Here, a cavity with wavy surface and flexible wall is studied. Figure 1 illustrates a model schematic along with the corresponding coordinate system. The model illustrates the instability of heat transfer and free convection within a Newtonian, incompressible liquid contained within a wavy vessel of length $L$ including a flexible right wall. Container's left wavy wall maintains a high isothermal temperature ($T_h$), whilst the flexible wall exhibits a lower temperature ($T_c$). The thermal insulation condition is preserved in the horizontal walls. As a result of Boussinesq's approximation and ignoring Joule heating effects, thermal insulation is obtained for horizontal walls. In accordance with Alsabery *et al.* (2019b), the dimensions primary equations can be articulated based on a set of assumptions in an arbitrary Lagrangian−Eulerian (ALE) formulation:

$$\nabla^* \cdot \mathbf{U}^* = 0, \tag{1}$$

$$\left(\frac{\partial \mathbf{U}^*}{\partial t} + (\mathbf{U}^* - \mathbf{W}^*) \cdot \nabla^* \mathbf{U}^*\right) = \left(\nu_f \nabla^{*2} \mathbf{U}^* - \beta \mathbf{g}(T_c - T) - \frac{1}{\rho_f} \nabla^* P^*\right), \tag{2}$$

$$\left(\frac{\partial T}{\partial t} + (\mathbf{U}^* - \mathbf{W}^*) \cdot \nabla^* T\right) = \alpha_f \nabla^{*2} T, \tag{3}$$

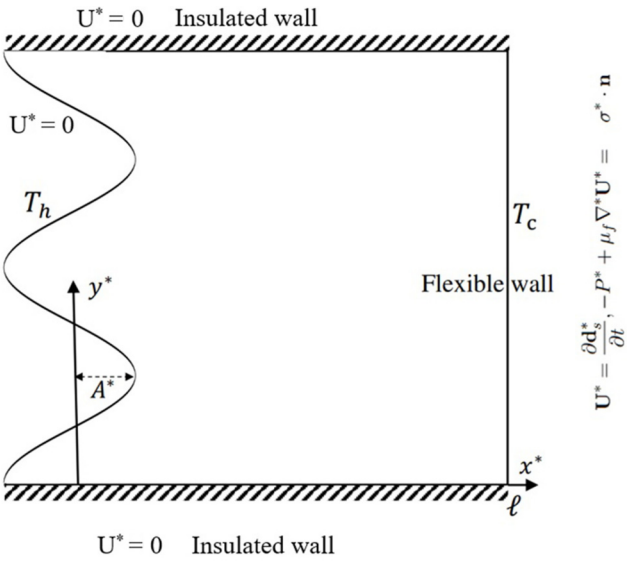


**Source(s):** Figure by authors

**Figure 1.** Schematic diagram of the square wavy container

here $\mathbf{U}^*$ represents velocity of the fluid while, and $\mathbf{W}^* = (U_s^*, V_s^*)$ represents moving mesh component velocities. $P^*$ and $T$, represent the pressure and temperature fields, respectively. Density, diffusivity, viscosity kinematics and thermal expansion, respectively, are represented by symbols $\rho_f$, $\alpha_f$, $\nu_f$ and $\beta$. An acceleration due to gravity is denoted by **g**.

A thin flexible wall is deflected using Mehryan *et al.* (2017):

$$\mathbf{F}_{\nu}^{*} = \left(\rho_s \frac{d^2\mathbf{d}_s^*}{dt^2} - \nabla^*\sigma^*\right). \tag{4}$$

The stress tensor, applied volumetric forces and the displacement of the wall structure, respectively, are represented by $\sigma^*$, $\mathbf{F}_{\nu}^{*}$ and $\mathbf{d}_s^*$. The wall structure's motion was simulated using a hyper-elastic model was applied, while the tension tensor was calculated by a Neo-Hookean formula:

$$\sigma^* = SJ^{-1}FF^T, \tag{5}$$

where

$$S = \frac{\partial W_s}{\partial \varepsilon},\ F = \left(\nabla^*\mathbf{d}_s^* + I\right),\ \text{and}\ \det(F) = J. \tag{6}$$

The transpose operation is indicated by $(T)$. $(\varepsilon)$ defines the strain, and $(W_s)$ defines the energy density as:

$$W_s = \left(-\mu_l ln\,(J) + \frac{1}{2}\lambda(ln\,(J))^2\right) + \frac{1}{2}\mu_l(J - I_l - 3), \tag{7}$$

$$\varepsilon = \frac{1}{2}\left(\left(\nabla^*\mathbf{d}_s^{*T}\nabla^*\mathbf{d}_s^*\right) + \nabla^*\mathbf{d}_s^* + \nabla^*\mathbf{d}_s^{*T}\right). \tag{8}$$

In this case, the first and second Lame constants can be expressed as $\mu_l = \frac{E_\tau}{2(1+\nu)}$ and $\lambda = \frac{E_\nu}{(1+\nu)(1-2\nu)}$, respectively. Here, $I_l$ represents deformation tensor Cauchy-Green's primary invariant. The Poisson's ratio and Young's modulus are denoted by $\nu$ and $E$, respectively. Furthermore, the boundary conditions were defined by the continuity of displacements and forces at the liquid-wall interface:

$$\mathbf{U}^* = \frac{\partial \mathbf{d}_s^*}{\partial t},\ -P^* + \mu_f\nabla^*\mathbf{U}^* = \sigma^* \cdot \mathbf{n} \tag{9}$$

Heat flux continuity and temperature were determined at the interface between the thin wall and the liquid:

$$\frac{\partial T}{\partial \mathbf{n}} = 0,\ T = T_c. \tag{10}$$

Here, **n** corresponds to the wall's normal vector.

Next, we introduce a set of nondimensional parameters:

$$\frac{x}{L}=X,\ \frac{y}{L}=Y,\ \frac{\mathbf{U}^*L}{\alpha_f}=\mathbf{U},\ \frac{\mathbf{W}^*L}{\alpha_f}=\mathbf{W},\ \frac{\nabla^*}{L}=\nabla,\ \frac{\nabla^{*2}}{L^2}=\nabla^2,$$
$$\theta=\frac{T-T_c}{T_h-T_c},\ \mathbf{d}_s=\frac{\mathbf{d}_s^*}{L},\ \sigma=\frac{\sigma^*}{E^*},\ t_p=\frac{t_p^*}{L^2},\ \tau=\frac{t\alpha_f}{L^2},\ P=\frac{L^2}{\rho_f\alpha_f^2}P^*, \tag{11}$$
$$\mathbf{F}_\nu^*=\frac{(\rho_f-\rho_s)Lg}{E_\nu},\ E=\frac{E_\nu L^2}{\rho_f\alpha_f^2},\ Ra=\frac{\mathbf{g}\beta_f\rho_f(T_h-T_c)L^3}{\mu_f\alpha_f},\ \rho_r=\frac{\rho_f}{\rho_s}.$$

As a result, the equations had no dimension as follows:

$$\frac{1}{\rho_r}\frac{d^2\mathbf{d}_s}{d\tau^2}-E\nabla\sigma=E\mathbf{F}_\nu, \tag{12}$$

$$\nabla\cdot\mathbf{U}=0, \tag{13}$$

$$\left(\frac{\partial\mathbf{U}}{\partial\tau}+(\mathbf{U}-\mathbf{W})\cdot\nabla\mathbf{U}\right)=(Pr\,Ra\theta+Pr\,\nabla^2\mathbf{U}-\nabla P), \tag{14}$$

$$\nabla^2\theta=\left(\frac{\partial\theta}{\partial\tau}+(\mathbf{U}-\mathbf{W})\cdot\nabla\theta\right). \tag{15}$$

The thermophysical ratios, $\rho_r=\frac{\rho_f}{\rho_s}$ and $\rho_r=\frac{\rho_f}{\rho_s}$ in the above expressions denote density and diffusivity, respectively, while $Pr=\frac{\nu_f}{\alpha_f}$ denotes Prandtl number. Furthermore, the buoyancy body force is ignored, so $\mathbf{F}_\nu=0$ due to its negligible impact on the structure.
The following are the dimensionless boundaries conditions:

$$\text{A wavy surface}:\ (-A\cos(2N\pi X)),\ (V=U=0),\ (\theta=1),\ 0\le Y\le 1, \tag{16}$$

$$\text{On the flexible wall}:\ (V=U=0),\ (\theta=0),\ (0\le Y\le 1),\ (0\le X\le 1) \tag{17}$$

$$\text{Horizontal bottom and top walls are adiabatic}:\ \left(\frac{\partial\theta}{\partial Y}=0\right),\ (V=U=0). \tag{18}$$

On the flexible surface, the boundary conditions are:

$$\mathbf{U}=\frac{\partial\mathbf{d}_s}{\partial\tau},\ \text{and}\ (-P+Pr\,\nabla\mathbf{U})=E\sigma\cdot\mathbf{n}. \tag{19}$$

Nusselt number ($Nu$) is a characteristic parameter of heat transfer, which represents how much heat is being transferred into the cavity. The surface energy balance allows us to calculate the rate of thermal transfer along a wavy surface, i.e. Nusselt's number (local):

$$Nu = -\frac{hL}{k} = -L\frac{\partial\theta}{\partial n}, \tag{20}$$

$$\frac{\partial\theta}{\partial n} = \sqrt{\left(\frac{\partial\theta}{\partial Y}\right)^2 + \left(\frac{\partial\theta}{\partial X}\right)^2}\frac{1}{L}. \tag{21}$$

By integrating over the Nusselt number, ($\overline{Nu}$), the cavity's mean heat transfer can be determined:

$$\overline{Nu} = \frac{1}{S}\int_0^S Nu\,\mathrm{d}S. \tag{22}$$

## 3. Methodologies for computation

A numerical solution is found for these dimensionless equations by using Galerkin weighted residual finite elements in equations (12)–(15) under initial and boundary conditions in equations (16)–(19). According to Figure 2, a triangular component has been discretized at various times within the computing region. Reddy (Reddy, 1993) describes in detail the finite element method procedure. Furthermore, for each of the existing variables, convergence toward the solution persists under these conditions:

$$\left|\frac{\Gamma^{i+1} - \Gamma^i}{\Gamma^{i+1}}\right| \leq 10^{-6}. \tag{23}$$

In case with $N = 3$, $E = 10^{12}$, $Ra = 10^7$ and $A = 0.1$, we performed calculations using a variety of grid sizes to verify that the current solver is independent of the computational domain grid size to determine the minimum strength of the mean Nusselt number ($\overline{Nu}$), and the flow circulation ($\Psi_{\min}$). According to Table 1, the G5 uniform grid shows negligible differences from the finer grids. This paper uses the G5 uniform grid to compute all similar problems.

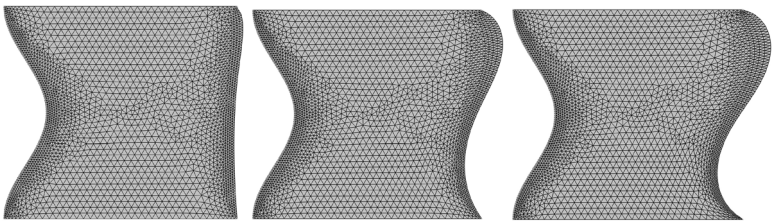

**Source(s):** Figure by authors

**Figure 2.** Grid-points distribution for a grid size 4969 at different time (left) $\tau = 0.001$, (middle) $\tau = 0.01$ and (right) $\tau = 1$

**Table 1.** Analyzing grids for $\Psi_{min}$ and $\overline{Nu}$ at several grid numbers for $N = 3$, $E = 10^{12}$, $A = 0.1$ and $Ra = 10^7$

| Item | Elements no. | $\Psi_{min}$ | $\overline{Nu}$ |
|---|---|---|---|
| G1 | 2773 | −41.638 | 19.961 |
| G2 | 3119 | −41.61 | 20.032 |
| G3 | 3439 | −40.564 | 20.192 |
| G4 | 4299 | −40.416 | 20.303 |
| **G5** | 4969 | −40.383 | 20.307 |
| G6 | 6499 | −40.374 | 20.311 |

**Source(s):** Table by authors

With the aim of validating the numerical results, comparisons are made using numerical and experiment data from Paroncini *et al.* (2012) based on free convection inside square enclosures surrounded by sidewalls, as shown in Figure 3. Besides, different validation does performed by comparing the results of the current study with the numerical findings of Mehryan *et al.* (2017) for convection and FSI models, within cavities divided by a flexible membrane for parameters $Ra = 10^7$, $Pr = 6.2$ and $E = 10^{14}$, as presented in Figure 4(a) and 4 (b), . Moreover, the results of the current overall heat transfer have been correlated with the numerical outcomes that described in Churchill (2002) study and the experimental findings of Nishimura *et al.* (1988) regarding free convection within cavities with temperature variation toward side partitions, as exhibited in Figure 5 when $Pr = 6.0$. These comparisons indicate that the intended goals are significantly aligned with those in previous studies.

## 4. Analysis and discussion of results

This work investigates the following specializations about the corresponding dimensionless combinations: waved surface amplitude, $0 \leq A \leq 0.2$, undulated surface number, $1 \leq N \leq 5$, Rayeigh number, $10^4 \leq Ra \leq 10^7$. Young's modulus is taken as $E = 10^{12}$.

Figures 6(a)–(j) and 7(a)–(j) depict streamline time versus temperature contours for $n = 2$, $E = 10^{12}$, $Ra = 10^7$ and $A = 0.2$. The early stage, that is, $\tau = 0.0001$, is characterized by a straightened cold elastic wall, with poor circulation of natural convection in the cavity. There is a large distance between streamlines. Figure 7 shows that all of the enclosure, except for a

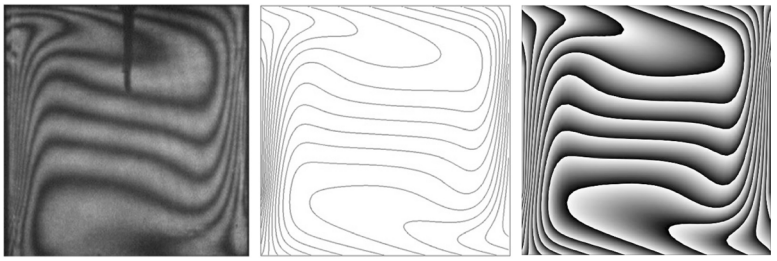

**Source(s):** Figure courtesy of Paroncini *et al.* (2012)

**Figure 3.** Comparison of isotherms between (left) experimental outcomes of Paroncini *et al.* (2012), (middle) numerical work of Paroncini *et al.* (2012) and (right) the current work; $Pr = 0.7$ and $Ra = 2.28 \times 10^5$

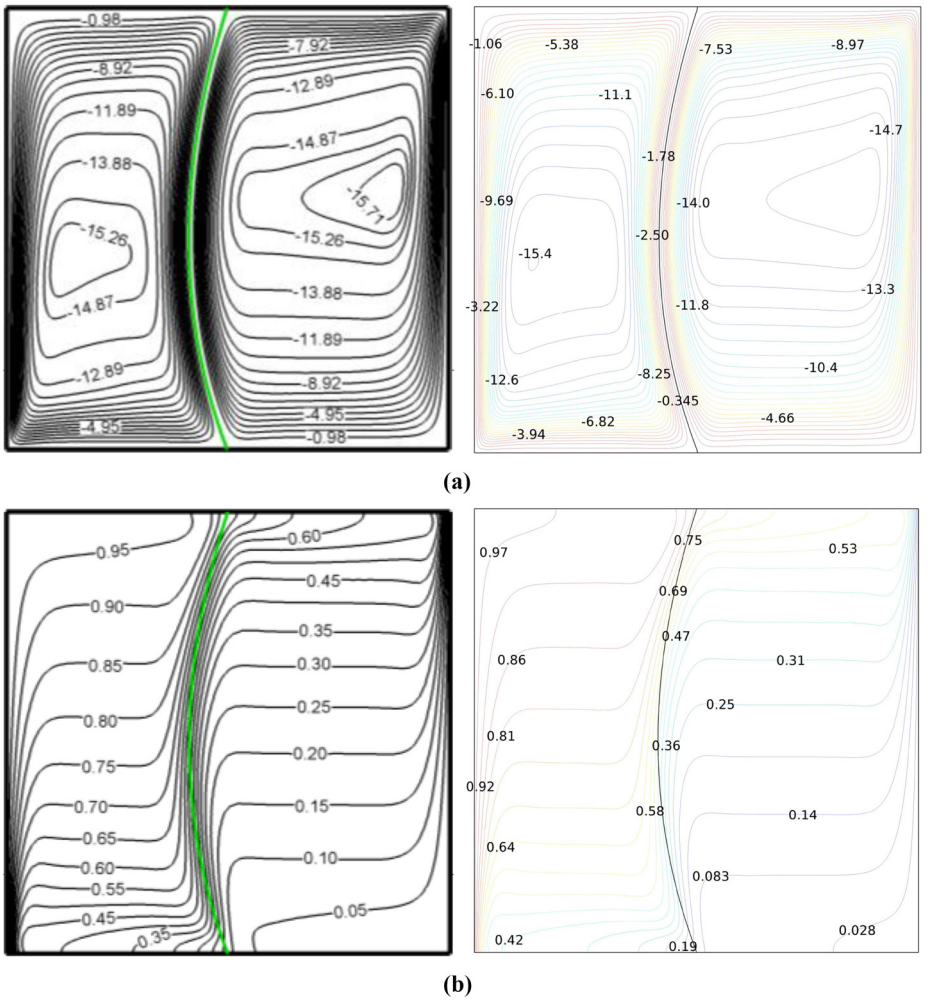


**Source(s):** Figure courtesy of Mehryan *et al.* (2017)

**Figure 4.** Streamlines (a) and isotherms (b); Mehryan *et al.* (2017) (left) and present study (right) for $Ra = 10^7$, $E = 10^{14}$ and $Pr = 6.2$

narrow area around the hot wall, is constant cold at the beginning ($\Theta = 0$). The plume of hot fluid shown in Figure 7(c) moves upward of the cavity because the cavity was initially at a low temperature. Heat causes the fluid's density to decrease, so buoyancy forces it upward as it moves up the hot wall. A deflection of the flexible wall is illustrated in Figure 7(c) at the upper right corner of the cavity. The hot fluid leaves the warm wall, moves up the top wall to reach the flexible wall. At corners, the fluid should switch direction to vertical from top to bottom. The flexible wall will therefore be subjected to a force that opposes the fluid's movement. As a consequence, the top wall appears concave. An intense natural convection

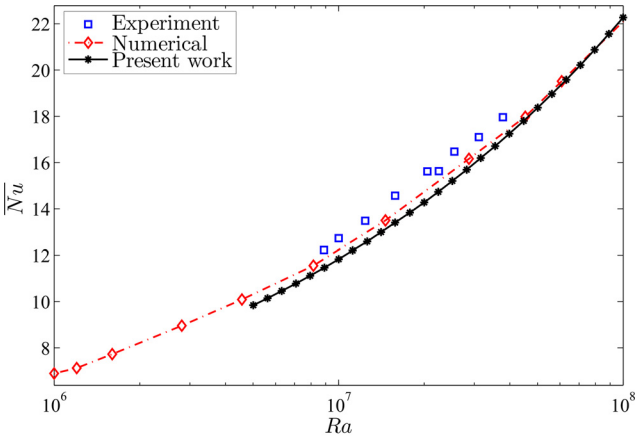


**Source(s):** Figure by authors

**Figure 5.** Comparison among the current overall Nusselt number and the experimental data confirmed by Nishimura *et al.* (1988) and the numerical outcome according to Churchill's relation by Churchill (2002) with Rayleigh number toward rectangular cavity at $AR = 4$ and $Pr = 6$

flow begins within the cavity after some time. Heat moves upward along the top wall until it reaches the flexible low-temperature wall. With the fluid near the cold wall moving downward, a loss of energy occurs as it moves toward the bottom. Figure 6(f) demonstrates a significant deflection of the flexible wall at the apex, resulting in a concave configuration. The streamlines of Figure 6(f) indicates that upon reaching the bottom, the cold fluid detaches from the cold wall. At its base, it creates a low-pressure zone as it exits cold walls. This low pressure causes flexible walls to gently incline inwards, resulting in convex shapes. Ultimately, the hole will remain invariant owing to the mass conservation. Consequently, the lower section of the flexible wall assumed a convex configuration to accommodate the overall volumetric alterations of the enclosure.

Figure 8(a)–(c) shows the steady-state temperature and streamline contours in the enclosures for $A = 0.2$, $E = 10^{12}$ and $Ra = 10^7$. Clearly, the undulation number is primarily affected by enclosure's core. The streamlines on the bottom and top walls behave similarly. Warm fluid ascends upward without regard to its configuration, after which the horizontal wall directs the fluid stream. In the same manner, as the cool fluid departs from cold walls, it passes through the bottom wall, flowing horizontally. Consequently, alterations in flexibility and number of undulations tend to be predominantly noticeable at the central regions of the enclosure. Figure 8 also shows that the amount of undulation has minimal impact on wall deflection. As mentioned, undulation number only affects the enclosure's core, whereas force exchanges primarily affect the cold wall's bottom and top. Therefore, the undulation number does not influence the flexibility of the wall. When the undulation number is small (lets say $N = 1,\ 2$), the fluid usually tracks the shape of the hot wall. However, when the undulation number reaches 3, the hot flow and streamlines follow the top wall rather than the corner. So, the contours of the isotherm can be seen to be affected by such a change in flow path.

For $E = 10^{12}$, $N = 4$ and $Ra = 10^7$, Figure 9(a)–(c) presents how the undulation amplitude affects the isotherms and streamlines. This figure shows that variations in undulation

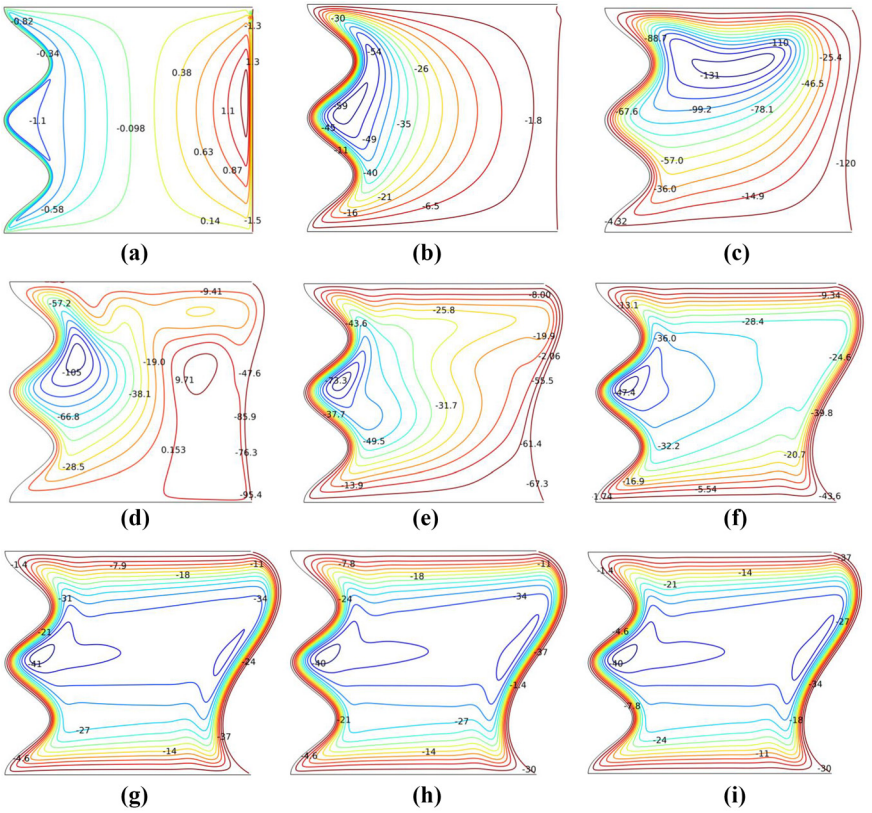


**Note(s):** (a) $\tau = 0.0001$; (b) $\tau = 0.0005$; (c) $\tau = 0.0015$; (d) $\tau = 0.003$; (e) $\tau = 0.006$; (f) $\tau = 0.02$; (h) $\tau = 0.06$; (i) $\tau = 0.1$; (j) $\tau = 1.0$
**Source(s):** Figure by authors

**Figure 6.** Time evolution of the streamlines at $N = 2$, $E = 10^{12}$, $A = 0.2$ and $Ra = 10^7$

amplitude have little effect on the overall behavior of isotherms and streamlines within the cavity, except close to the hot cavity wall. Due to the hot wavy wall, hot fluid streams through the wavy wall upwards. According to the hot wall isotherms, the hot wall is always covered with a layer of hot fluid regardless of the amplitude of the undulations. As this layer gets heated, it moves upward. A high undulation number dampens the hydraulic impact of the hot wall by covering it with a heated layer of liquid. In the case of a heated layer covering the wall, the effect of undulation amplitude on hydraulic behavior is minimal. Convection is also responsible for driving the process. Due to the increased buoyancy force caused by heat absorption in undulation space, the undulation amplitude has little effect on enclosure behavior in general. Heat transfer may increase as the gap between the cold and hot walls decreases as the undulation amplitude increases.

For $E = 10^{12}$, $N = 5$ and $A = 0.1$, Figure 10(a)–(c) illustrates Rayleigh numbers' consequences for streamlines and isotherms in steady-state conditions. In low Rayleigh numbers, flow circulation becomes poor, as the exchange of momentum between fluid flow and flexible walls remains limited. Accordingly, Figure 10(a) and (b), show that the cold wall

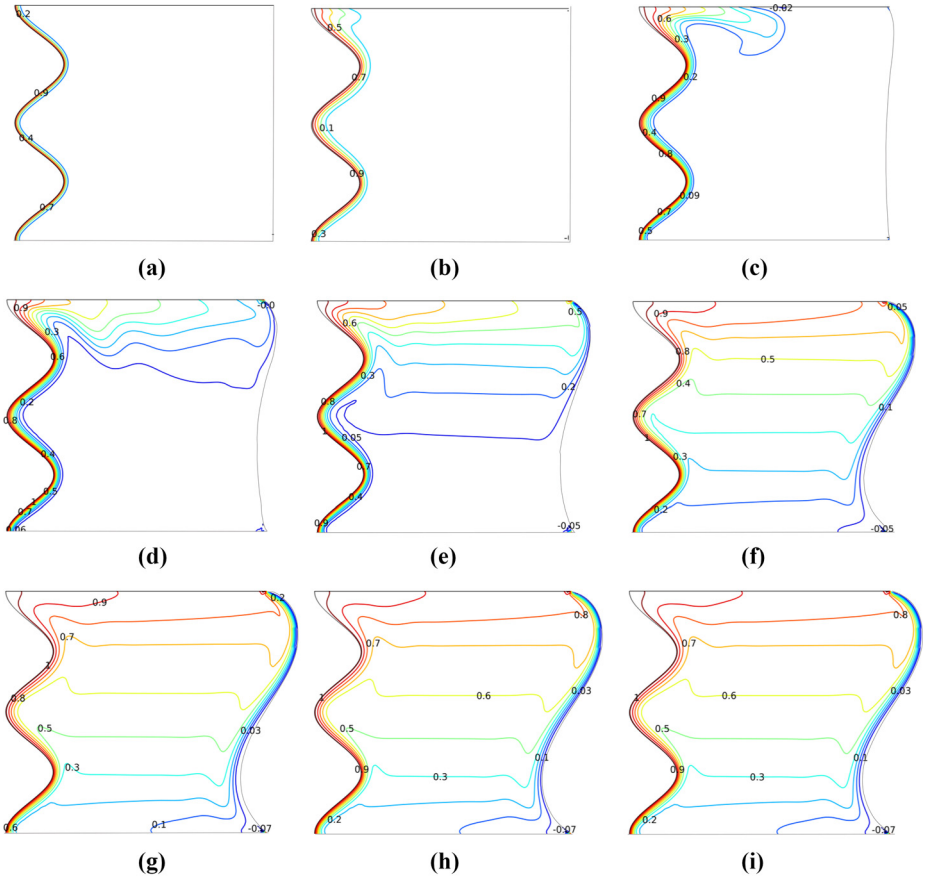


**Note(s):** (a) τ = 0.0001; (b) τ = 0.0005; (c) τ = 0.0015; (d) τ = 0.003; (e) τ = 0.006; (f) τ = 0.02; (h) τ = 0.06; (i) τ = 0.1; (j) τ = 1.0
**Source(s):** Figure by authors

**Figure 7.** Time evolution of the isotherms at $N = 2$, $E = 10^{12}$, $A = 0.2$ and $Ra = 10^6$

does not deflect much. As shown by the isotherms, streamlines do not pass through undulations with low Rayleigh numbers, thus keeping fluid trapped inside. In cases where Rayleigh numbers are high, fluid tends to penetrate into undulation spaces, thus proving the advantages of flexible and wavy walls.

Figure 11(a) and (b), illustrate how undulation number and amplitude affect local Nusselt number. Figure 11(a), plots the results along the wall's normal length. Hence, the wall's length will rise as the undulation number increases. Based on Figure 11(a), it can be seen that a substantial heat transfer occurs by convection from the wall's bottom, regardless of the undulations. In general, the Nusselt number decreases as distance increases from the bottom wall and as cold fluid approaches the wall. Due to the wavy geometry of the hot wall, the Nusselt number increases near geometrical waves over the warm wall. This is the point at which the wall is in contact with a fresh, cold flowing fluid. There is usually a trapped fluid

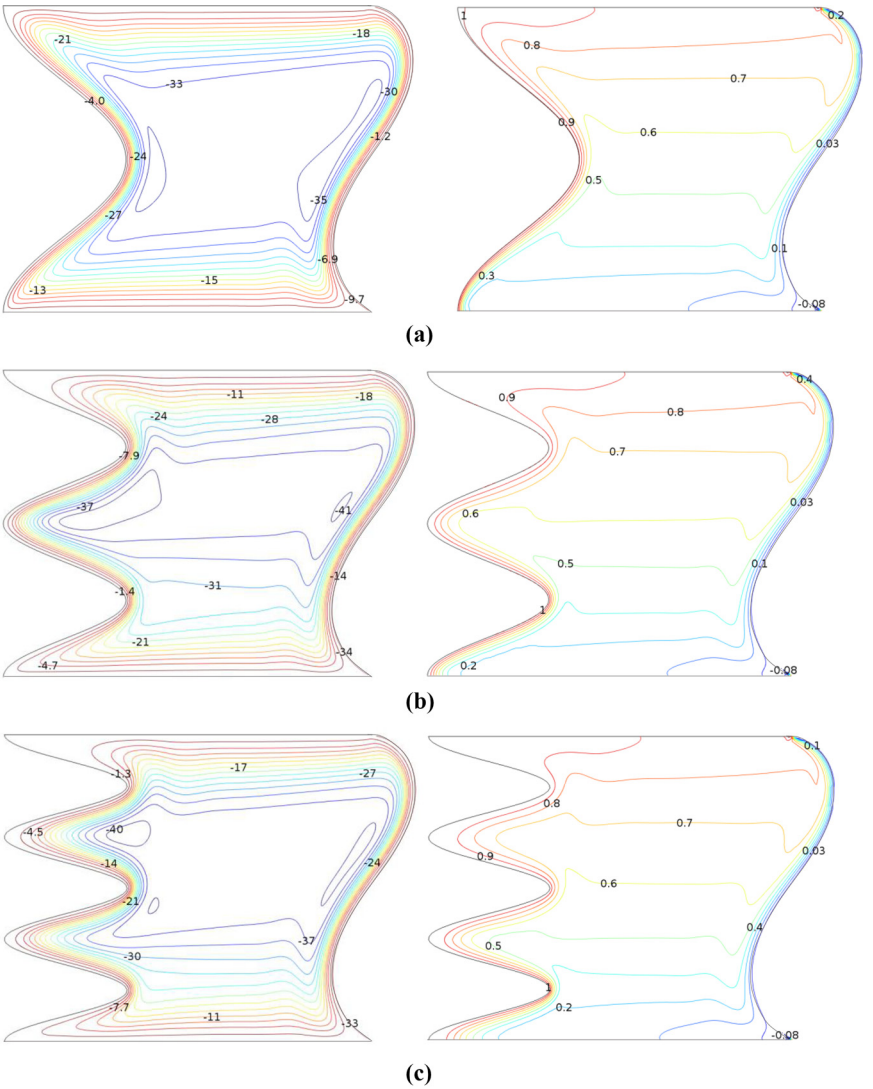


**Note(s):** (a) $N = 1$; (b) $N = 3$; (c) $N = 3$
**Source(s):** Figure by authors

**Figure 8.** Variation of the streamlines (left) and isotherms (right) evolution by undulation number for $E = 10^{12}$, $A = 0.2$ and $Ra = 10^7$

between the peaks in the undulation spaces and reaches a hot temperature between the peaks. As a result of this, the trapped fluid within the undulations has little temperature gradient. It is interesting to note that at the left undulation peaks, which are quite enclosed within a hot uniform fluid, the minimum local Nusselt number equals zero. In addition, maximum

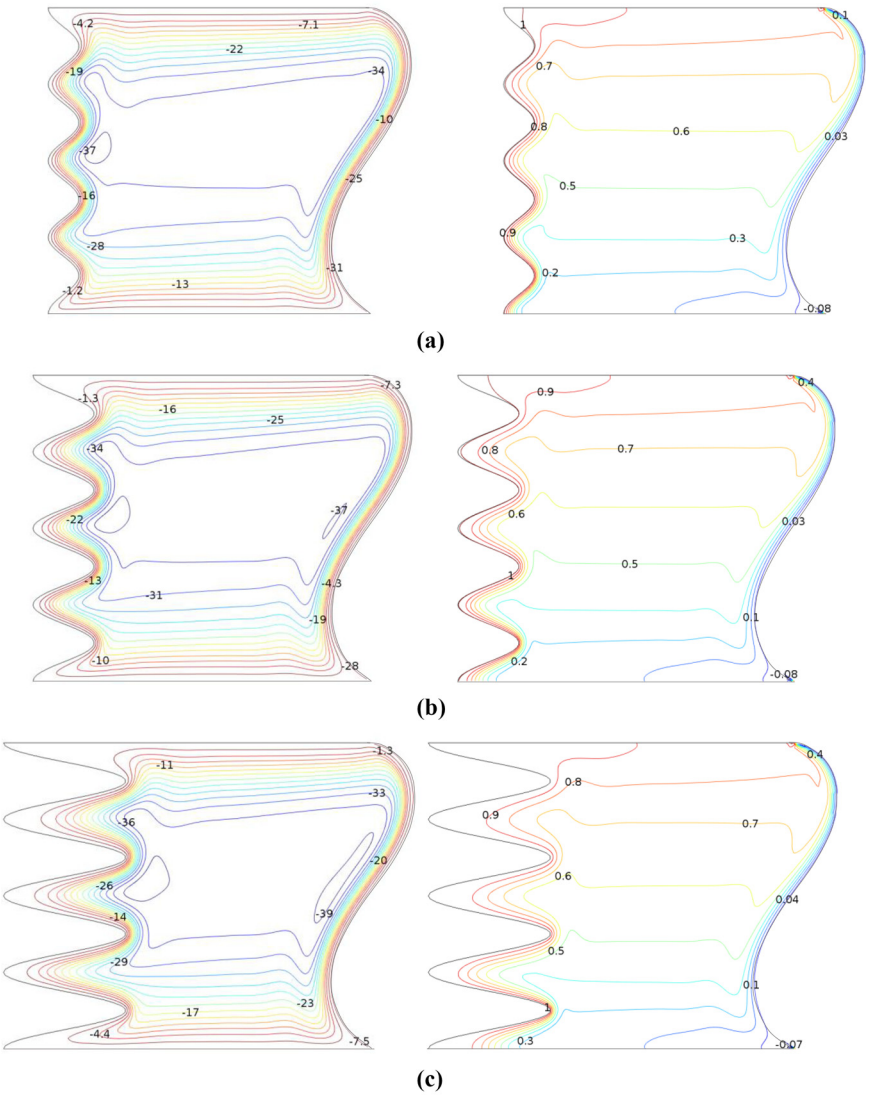


**Note(s):** (a) $A = 0.05$; (b) $A = 0.1$; (c) $A = 0.2$
**Source(s):** Figure by authors

**Figure 9.** Variation of the streamlines (left) and isotherms (right) evolution by undulation amplitude for $E = 10^{12}$, $N = 4$ and $Ra = 10^7$

Nusselt number peaks $N = 4$ are comparable with that of $N = 5$. The increase of the undulation amplitude extends the overall hot wall length, and hence, the larger the undulation amplitude, the longer the wall length. A small undulation amplitude results in large maximum local Nusselt number at the inside undulation peaks and also larger values of

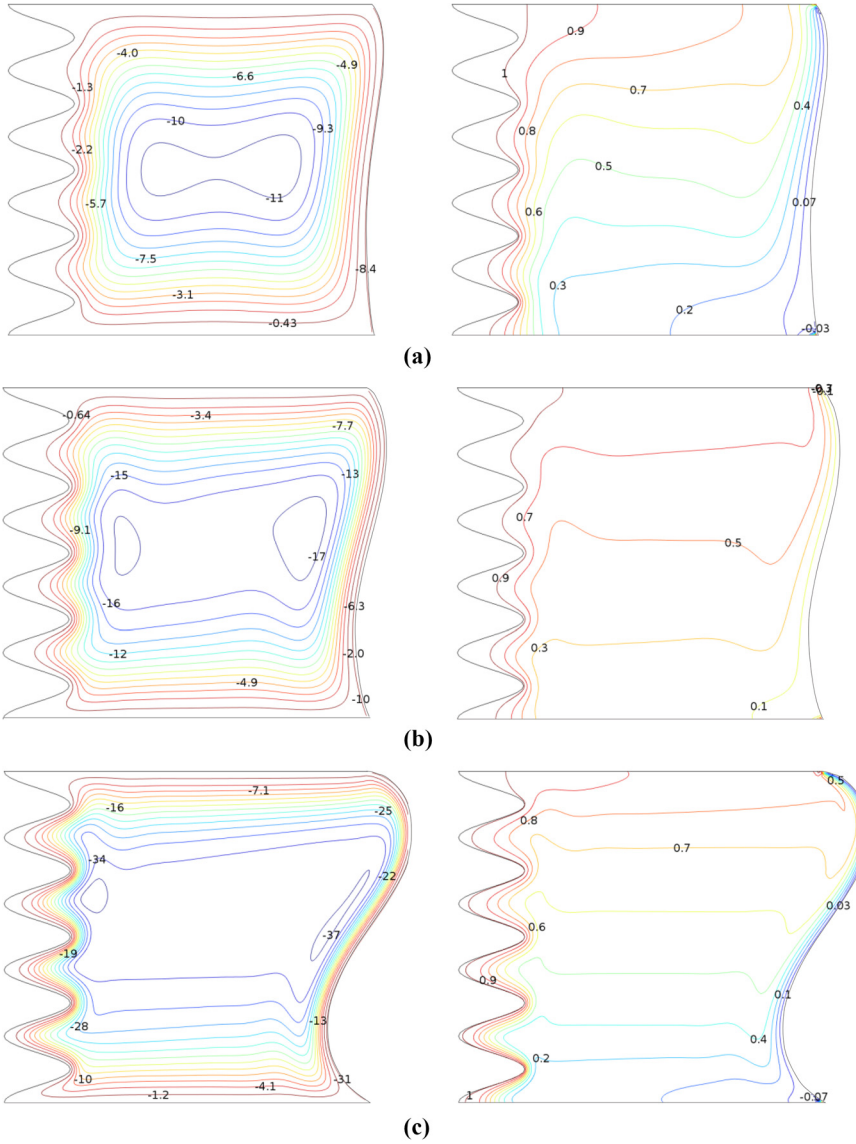


**Note(s):** (a) $Ra = 1.3 \times 10^5$; (b) $Ra = 7.5 \times 10^5$; (a) $Ra = 10^7$
**Source(s):** Figure by authors

**Figure 10.** Variation of the streamlines (left) and isotherms (right) evolution by Rayleigh number for $E = 10^{12}$, $N = 5$ and $A = 0.1$

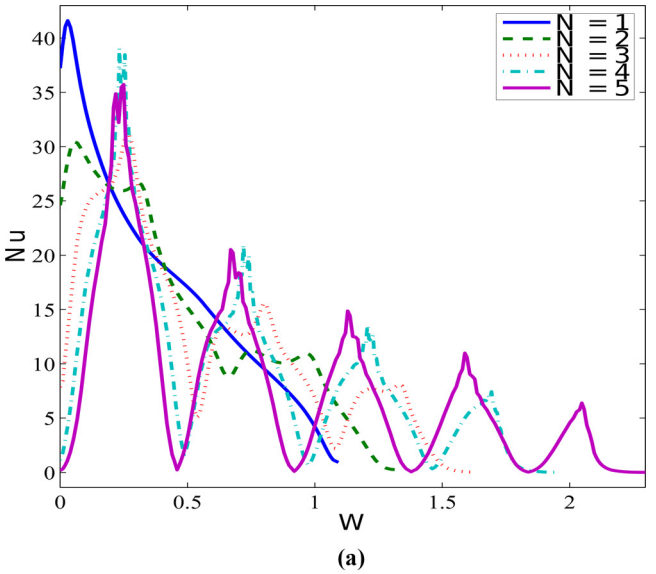


**Note(s):** (a) $A = 0.1$; (b) $N = 5$
**Source(s):** Figure by authors

**Figure 11.** Variation of local *Nu* along the left wall for different undulation number (a) and undulation amplitude (b) at $Ra = 10^7$ and $E = 10^{12}$

minimum local Nusselt numbers at the outside undulation peaks. This is since a small undulation amplitude does not trap the fluid. A small undulation amplitude, however, could result in a shorter overall wall-length, thereby reducing the overall thermal transfer rate, i.e. average Nusselt.

Figure 12 illustrates the mean Nusselt number over the time period for various numbers 12(a) and undulation amplitudes 12(b) at $E = 10^{12}$ and $Ra = 10^7$. As seen in this figure, the undulation number and amplitudes are significant at an early stage. Undulation amplitudes and undulation numbers affect average Nusselt numbers moderately during transitional phases, while undulation numbers have a small effect. By adjusting undulation amplitudes, the transitional phase interval can be shifted. Figure 11 shows the influence of undulation amplitudes and undulation numbers on mean Nusselt numbers during steady phases. As discussed in previous figures, this conclusion is consistent with streamline and isotherm contours.

In Figure 13, Rayleigh number is examined in relation to Nusselt number for the cases of $N = 1$ 13(a), and $N = 5$ 13(b). Figure 13(a) depicts a local maximum for Nusselt number at $N = 1$. With $Ra = 10^4$, the flow circulation is weak, and the conduction effects are important. According to Figure 8, the shortest distance exists midway along the hot wall's length. Nusselt number reaches its maximum here. As Rayleigh number increases, convection flows become stronger, diminishing this local conduction advantage. A higher Rayleigh number corresponds to a higher Nusselt number overall. Figure 13(b), shows how increasing Rayleigh number increases undulation's effect on streamlines. This is in agreement with the discussion of Figure 10, where the same conclusion was achieved from the distribution of the streamlines. Interestingly, increasing Rayleigh numbers reduces the length of minimum Nusselt numbers. Nusselt number minimums occur in areas where hot fluid traps are small and gradients in temperatures are small. By increasing Rayleigh number, streamlines enter the undulation spaces, and the trapped regions decline.

Figure 14 illustrates the mean Nusselt number over time at different Rayleigh numbers for $N = 1$ [Figure 14(a)] and $N = 5$ [Figure 14(b)]. The development of convection heat transfer progresses through three distinct phases: The initial phase between $0.0001 < \tau < 0.001$, a transition phase between $0.001 < \tau < 0.1$ and then a steady state after $\tau = 0.1$ for a Rayleigh number of $Ra = 10^6$. Phase intervals can be adjusted by modifying the Rayleigh number. In both figures, Rayleigh number fluctuations are observed during the initial phase. These fluctuations result from changes in the flexible wall shape. As the Rayleigh number increases, more pronounced fluctuations are noted during the transitional phase. In the steady phase, convection becomes significantly more intense at higher Rayleigh numbers, particularly in both the one undulation and $N = 5$ cases.

An analysis of the effect of the undulation amplitude (Figure 15) as well as the undulation number (Figure 16) on the mean Nusselt number can be seen in Figures 15 and 16. Here, Figure 15(a) shows the results for the case of $N = 1$, while Figure 15(b) is plotted for $N = 5$. The increase in undulation amplitude improves the mean Nusselt number for Rayleigh numbers that are large; however, when the Rayleigh number is low, the variation undulation amplitude has little effect. This improvement could be attributed to the hot wall's increased length. However, in the case of $N = 5$, an opposite behavior could be observed. As the undulation amplitude increases, the mean Nusselt number is reduced. As the undulation increases in amplitude, the hot wall lengthens, but trapped regions increase too, where the hot fluid accumulates without contributing to transferring heat. The mean Nusselt number generally deteriorates with increasing the undulation number when the undulation amplitude is moderate, i.e. $A = 0.1$ in Figure 16. There are fee expectations at high Rayleigh numbers about $10^7$ where the circulation flow gets quite intense and penetrates the trapped regions between undulations.

Figure 17 shows the steady-state mean Nusselt number at $Ra = 10^7$ and $E = 10^{12}$ as a function of undulation amplitude and number. The Nusselt number increases with the undulation number up to $N = 3$, with a 4.7% improvement from 18.1 to 19.0, when the

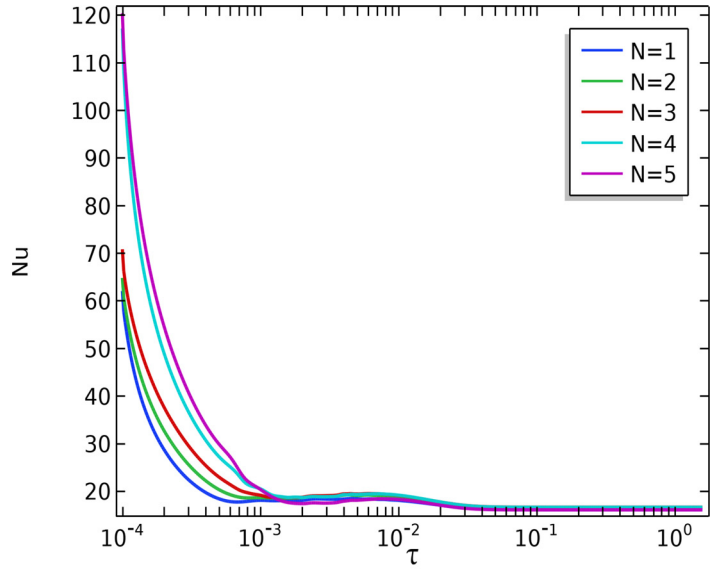


**(a)**

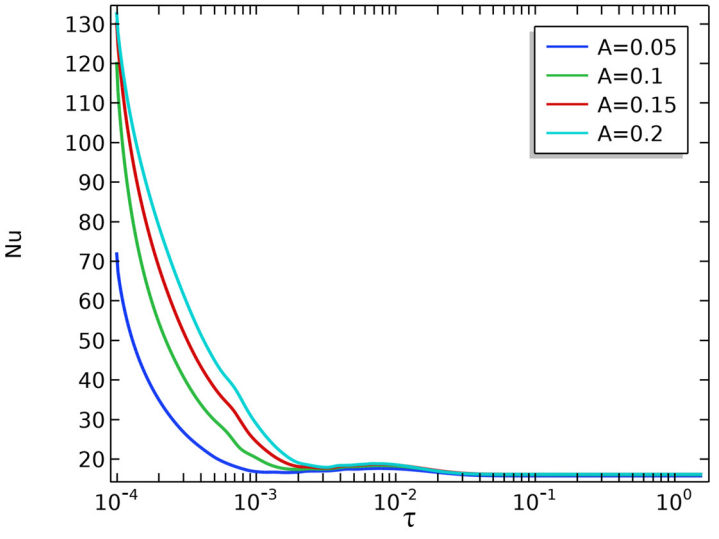


**(b)**

**Note(s):** (a) $A = 0.1$; (b) $N = 5$
**Source(s):** Figure by authors

**Figure 12.** Variation of the unsteady $\overline{Nu}$ with $\tau$ for different $N$ (a) and $A$ (b) at $E = 10^{12}$ and $Ra = 10^7$

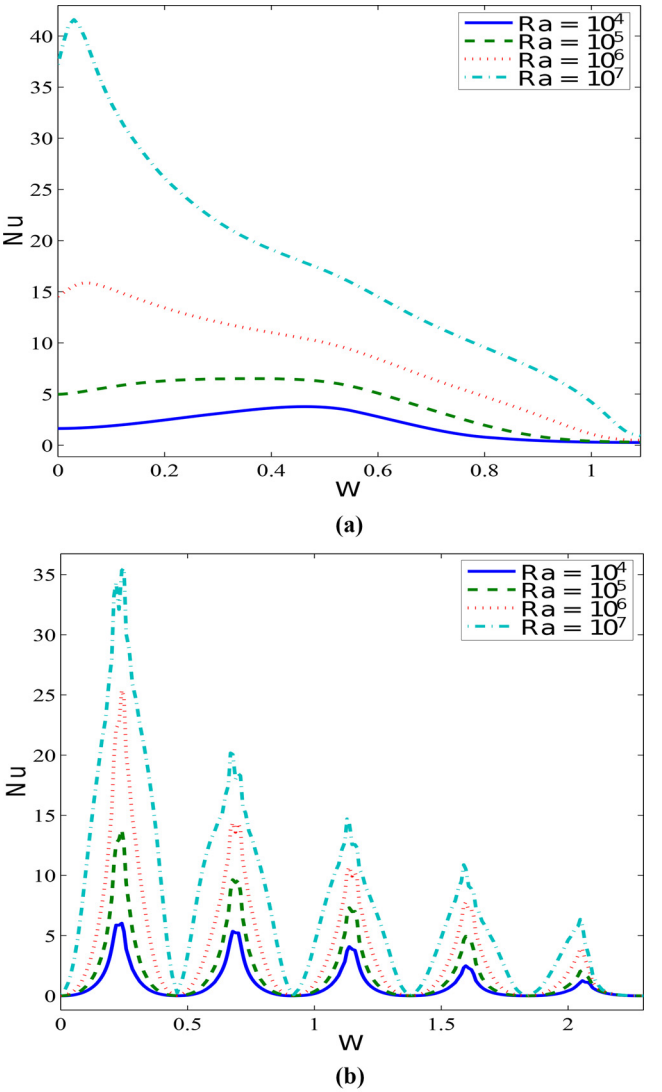


**Source(s):** Figure by authors

**Figure 13.** Variation of local *Nu* along the left wall for different *Ra* when undulated number, $N = 1$ (a) and undulated number, $N = 5$ (b) at $A = 0.1$ and $E = 10^{12}$

number of undulations increases from 1 to 3 for an amplitude of $A = 0.15$. Further increases in undulation number reduce the Nusselt number due to fluid trapping in closely spaced undulations, limiting temperature gradients and heat transfer. In addition, increasing the undulation amplitude from 0.05 to 0.20 at $N = 3$ results in an 8.8% improvement, raising the Nusselt number from 17.6 to 19.3. Thus, the optimum heat

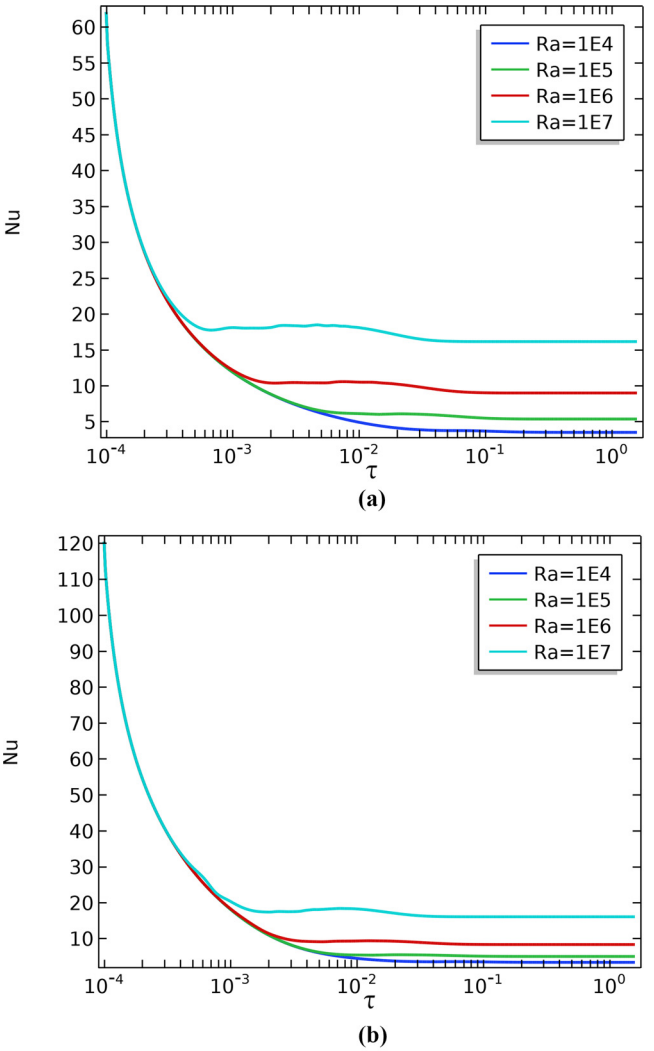


**Source(s):** Figure by authors

**Figure 14.** Variation of the unsteady $\overline{Nu}$ with $\tau$ for different $Ra$ when $N = 1$ (a) and $N = 5$ (b) at $A = 0.1$ and $E = 10^{12}$

transfer is achieved with $N = 3$ and $A = 0.20$, balancing enhanced heat transfer surface area with fluid circulation.

Table 2 shows the average Nusselt number for both flexible ($E = 10^{12}$) and rigid walls across different wavy amplitudes ($A$) and wavy numbers ($N$). The results demonstrate that flexible walls consistently improve the heat transfer rate, as seen by the higher average Nusselt numbers compared to rigid walls. The greatest enhancement in heat transfer occurs at three undulations ($N = 3$) and larger amplitudes ($A = 0.15$ and $A = 0.2$), where the Nusselt

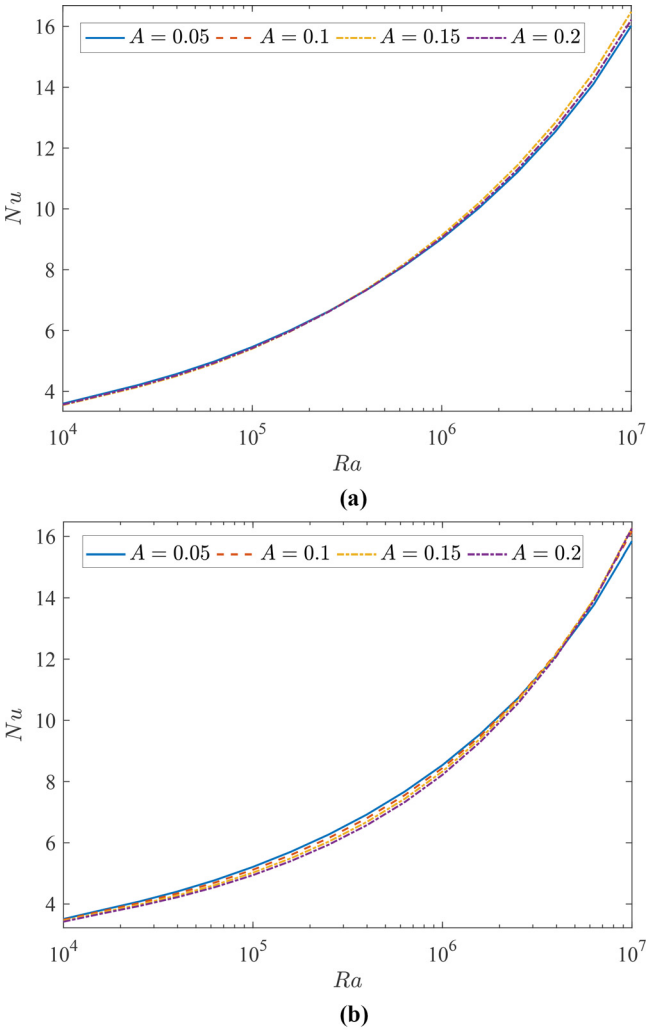


**Source(s):** Figure by authors

**Figure 15.** Variation of $\overline{Nu}$ with $Ra$ for different $A$ when (a) $N = 1$ and (b) $N = 5$ for $E = 10^{12}$

number reaches its peak values. This suggests that increasing the wavy amplitude and undulation number can significantly boost heat transfer, especially when using flexible walls. However, at higher undulation numbers ($N = 5$), the heat transfer enhancement decreases, indicating that there may be an optimal range for maximizing performance.

## 5. Conclusions

This study examined FSIs in natural convection within a wavy enclosure featuring right-movable walls. The governing partial differential equations are numerically solved by

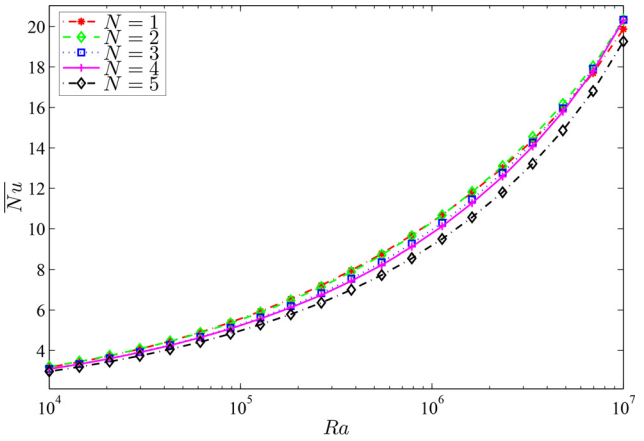


**Source(s):** Figure by authors

**Figure 16.** Variation of $\overline{Nu}$ with $Ra$ for different $N$ when undulation amplitude, $A = 0.1$ at $E = 10^{12}$

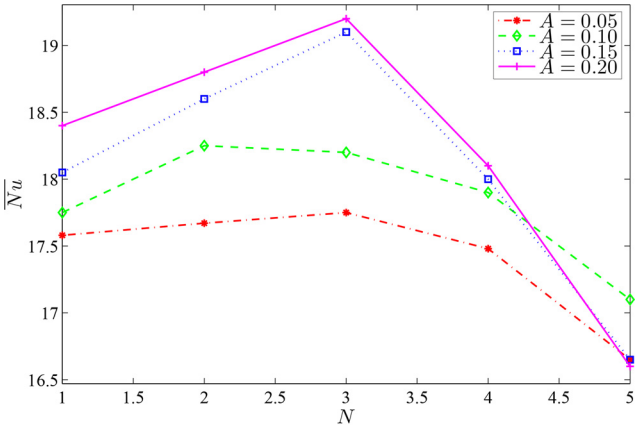


**Source(s):** Figure by authors

**Figure 17.** Variation of $\overline{Nu}$ with $N$ for different $N$ when Rayleigh number, $Ra = 10^7$ at $E = 10^{12}$

applying the Galerkin finite element technique. The simulation findings concerning temperature and flow distributions, along with overall thermal transfer, are represented graphically. The waviness, Rayleigh number and elasticities are intricately linked to the design of streamline vortices, thermal patterns and modes of heat transport. As a result of the current investigation, the following notable findings were found:

- Structural deformation of wavy-heated walls extremely improves heat transfer performance by inducing complex flow patterns, which enable greater thermal mixing.

**Table 2.** The variations of the average Nusselt ($\overline{Nu}$) number with the flexible and rigid wall for various values of the waviness parameter

| Elasticity and waviness parameters | $N = 1$ | $N = 3$ | $N = 5$ |
|---|---|---|---|
| Flexible, $A = 0.05$ | 17.58 | 17.75 | 16.65 |
| Rigid, $A = 0.05$ | 16.02 | 16.51 | 14.99 |
| Flexible, $A = 0.1$ | 17.75 | 18.24 | 17.12 |
| Rigid, $A = 0.1$ | 15.98 | 16.78 | 15.24 |
| Flexible, $A = 0.15$ | 18.05 | 19.11 | 16.65 |
| Rigid, $A = 0.15$ | 15.88 | 17.19 | 14.49 |
| Flexible, $A = 0.2$ | 18.41 | 19.25 | 16.62 |
| Rigid, $A = 0.2$ | 15.83 | 16.88 | 14.23 |

**Source(s):** Table by authors

- The composite impact of wall waviness and elasticity greatly impacts the natural convection characteristics within the enclosure, influencing both the rate of heat transfer and flow of fluids.
- The transfer of heat by convection occurs in three phases: initial, transitional and a steady state. The intervals of each phase can be altered by changing the undulation amplitude, and the Rayleigh number.
- A number of factors influence the thermal design and formation of circulation flow, including Rayleigh number, wall flexibility, amplitude and undulations. Changes in the undulation number and flexible wall can have a notable impact, especially in the core regions and near the hot wall.
- One and two undulation at large amplitude and high Rayleigh number cases penetrated toward improved heat transfer and the appearance of flexible surfaces.
- Increasing the undulation amplitude from 0.05 to 0.20 at $N = 3$ improves the average Nusselt number from 17.6 to 19.3, an 8.8% increase in heat transfer. With a typical amplitude of $A = 0.15$, increasing the undulation number from 1 to 3 raises the average Nusselt number from 18.1 to 19.0, a 4.7% improvement in heat transfer.
- The understandings achieved from this study on the interplay between wall waviness and elasticity can be used to design of more efficient techniques in energy management, microfluidics and other engineering specializations where natural convection and flexible boundaries are crucial.

## References

Abdelkader, S., Mébrouk, R., Abdellah, B. and Khadidja, B. (2007), "Natural convection in a horizontal wavy enclosure", *Journal of Applied Sciences*, Vol. 7 No. 3, pp. 334-341.

Adjlout, L., Imine, O., Azzi, A. and Belkadi, M. (2002), "Laminar natural convection in an inclined cavity with a wavy wall", *International Journal of Heat and Mass Transfer*, Vol. 45 No. 10, pp. 2141-2152.

Ahmed, A.Q. and Razavi, S.E. (2024), "Enhancing heat transfer in L-shaped enclosures with combined natural convection-fluid structure interaction: incorporating flexible fin and elastic wall", *Numerical Heat Transfer, Part A: Applications*, pp. 1-27.

Al-Amiri, A. and Khanafer, K. (2011), "Fluid-structure interaction analysis of mixed convection heat transfer in a lid-driven cavity with a flexible bottom wall", *International Journal of Heat and Mass Transfer*, Vol. 54 Nos 17/18, pp. 3826-3836.

Alazzam, A., Qasem, N.A., Aissa, A., Abid, M.S., Guedri, K. and Younis, O. (2023), "Natural convection characteristics of nano-encapsulated phase change materials in a rectangular wavy enclosure with heating element and under an external magnetic field", *Journal of Energy Storage*, Vol. 57, p. 106213.

Alrasheedi, N.H. (2024), "Analysis of fluid-structure interaction in the transfer of heat through natural convection within a L-shaped wavy enclosure featuring a movable baffle", *Journal of Engineering Research.*

Alsabery, A., Ismael, M., Chamkha, A. and Hashim, I. (2018), "Numerical investigation of mixed convection and entropy generation in a wavy-walled cavity filled with nanofluid and involving a rotating cylinder", *Entropy*, Vol. 20 No. 9, p. 664.

Alsabery, A., Saleh, H., Ghalambaz, M., Chamkha, A. and Hashim, I. (2019a), "Fluid-structure interaction analysis of transient convection heat transfer in a cavity containing inner solid cylinder and flexible right wall", *International Journal of Numerical Methods for Heat and Fluid Flow*, Vol. 29 No. 10, pp. 3756-3780.

Alsabery, A., Selimefendigil, F., Hashim, I., Chamkha, A. and Ghalambaz, M. (2019b), "Fluid-structure interaction analysis of entropy generation and mixed convection inside a cavity with flexible right wall and heated rotating cylinder", *International Journal of Heat and Mass Transfer*, Vol. 140, pp. 331-345.

Borah, A., Mehta, S.K. and Pati, S. (2023), "Analysis of conjugate heat transfer for forced convective flow through wavy minichannel", *International Journal of Numerical Methods for Heat and Fluid Flow*, Vol. 33 No. 1, pp. 174-203.

Chattopadhyay, A., Pandit, S. and Oztop, H. (2020), "An analysis of thermal performance and entropy generation in a wavy enclosure with moving walls", *European Journal of Mechanics - B/Fluids*, Vol. 79, pp. 12-26.

Cho, C. (2019), "Mixed convection heat transfer and entropy generation of Cu-water nanofluid in wavy-wall lid-driven cavity in presence of inclined magnetic field", *International Journal of Mechanical Sciences*, Vol. 151, pp. 703-714.

Churchill, S.W. (2002), "Free convection in layers and enclosures", in Hewitt, G.f (Ed.), *Heat Exchanger Design Handbook*, section 258, Begell House, New York, NY.

Das, P. and Mahmud, S. (2003), "Numerical investigation of natural convection inside a wavy enclosure", *International Journal of Thermal Sciences*, Vol. 42 No. 4, pp. 397-406.

Dogonchi, A., Hashemi, T., Waqas, M., Seyyedi, S., Animasaun, I. and Ganji, D. (2020), "The influence of different shapes of nanoparticle on Cu-H2O nanofluids in a partially heated irregular wavy enclosure", *Physica A: Statistical Mechanics and Its Applications*, Vol. 540, p. 123034.

Engel, M. and Griebel, M. (2006), "Flow simulation on moving boundary-fitted grids and application to fluid-structure interaction problems", *International Journal for Numerical Methods in Fluids*, Vol. 50 No. 4, pp. 437-468.

Ghalambaz, M., Mehryan, S.A.M., Feeoj, R., Hajjar, A., Hashim, I. and Mahani, R. (2020), "Free convective heat transfer of a non-Newtonian fluid in a cavity containing a thin flexible heater plate: an Eulerian–Lagrangian approach", *Journal of Thermal Analysis and Calorimetry*, Vol. 147 No. 2, pp. 1-16.

Ghalambaz, M., Mehryan, S.A.M., Ismael, M.A., Chamkha, A. and Wen, D. (2019), "Fluid-structure interaction of free convection in a square cavity divided by a flexible membrane and subjected to sinusoidal temperature heating", *International Journal of Numerical Methods for Heat and Fluid Flow*, Vol. 30 No. 6.

Hasan, M., Saha, S. and Saha, S. (2012), "Effects of corrugation frequency and aspect ratio on natural convection within an enclosure having sinusoidal corrugation over a heated top surface", *International Communications in Heat and Mass Transfer*, Vol. 39 No. 3, pp. 368-377.

Hashemi, S., Armaghani, T. and Ghasemiasl, R. (2024), "3D numerical study of $Al_2O_3$-water nanofluid unsteady natural convection via using oscillating plate by two-way FSI analysis", *Journal of Thermal Analysis and Calorimetry*, Vol. 149 No. 17, pp. 9715-9730.

Hashim, I., Alsabery, A., Sheremet, M. and Chamkha, A. (2018), "Numerical investigation of natural convection of $Al_2O_3$-water nanofluid in a wavy cavity with conductive inner block using Buongiorno's two-phase model", *Advanced Powder Technology.*

Hussain, S. and Mohammed, R. (2011), "Effects of out of phase and inclination angles on natural convection heat transfer flow of air inside a sinusoidal corrugated enclosure with spatially variable wall temperature", *Journal of Enhanced Heat Transfer*, Vol. 18 No. 5, pp. 403-417.

Jamesahar, E., Ghalambaz, M. and Chamkha, A. (2016), "Fluid-solid interaction in natural convection heat transfer in a square cavity with a perfectly thermal-conductive flexible diagonal partition", *International Journal of Heat and Mass Transfer*, Vol. 100, pp. 303-319.

Jiang, X., Hatami, M., Abderrahmane, A., Younis, O., Makhdoum, B.M. and Guedri, K. (2023), "Mixed convection heat transfer and entropy generation of MHD hybrid nanofluid in a cubic porous cavity with wavy wall and rotating cylinders", *Applied Thermal Engineering*, Vol. 226, p. 120302.

Khanafer, K. (2014), "Comparison of flow and heat transfer characteristics in a lid-driven cavity between flexible and modified geometry of a heated bottom wall", *International Journal of Heat and Mass Transfer*, Vol. 78, pp. 1032-1041.

Khanafer, K. (2013), "Fluid-structure interaction analysis of non-Darcian effects on natural convection in a porous enclosure", *International Journal of Heat and Mass Transfer*, Vol. 58 No. 1-2, pp. 382-394.

Khanafer, K., Bull, J. and Berguer, R. (2009), "Fluid-structure interaction of turbulent pulsatile flow within a flexible wall axisymmetric aortic aneurysm model", *European Journal of Mechanics - B/Fluids*, Vol. 28 No. 1, pp. 88-102.

Mahmud, S., Das, P., Hyder, N. and Islam, A. (2002), "Free convection in an enclosure with vertical wavy walls", *International Journal of Thermal Sciences*, Vol. 41 No. 5, pp. 440-446.

Mahmud, S. and Fraser, R. (2004), "Free convection and entropy generation inside a vertical inphase wavy cavity", *International Communications in Heat and Mass Transfer*, Vol. 31 No. 4, pp. 455-466.

Mahmud, S. and Islam, A. (2003), "Laminar free convection and entropy generation inside an inclined wavy enclosure", *International Journal of Thermal Sciences*, Vol. 42 No. 11, pp. 1003-1012.

Mehryan, S.A.M., Alsabery, A., Modir, A., Izadpanahi, E. and Ghalambaz, M. (2020a), "Fluid-structure interaction of a hot flexible thin plate inside an enclosure", *International Journal of Thermal Sciences*, Vol. 153, p. 106340.

Mehryan, S.A.M., Ghalambaz, M., Feeoj, R., Hajjar, A. and Izadi, M. (2020b), "Free convection in a trapezoidal enclosure divided by a flexible partition", *International Journal of Heat and Mass Transfer*, Vol. 149, p. 119186.

Mehryan, S.A.M., Ghalambaz, M., Ismael, M. and Chamkha, A. (2017), "Analysis of fluid-solid interaction in MHD natural convection in a square cavity equally partitioned by a vertical flexible membrane", *Journal of Magnetism and Magnetic Materials*, Vol. 424, pp. 161-173.

Morsi, Y. and Das, S. (2003), "Numerical investigation of natural convection inside complex enclosures", *Heat Transfer Engineering*, Vol. 24 No. 2, pp. 30-41.

Nadeem, S., Salma, R., Ullah, N., Alzabut, J. and Ghazwani, H.A. (2023), "Numerical solutions for MHD mixed convection flow in a square wavy cavity inside heated corrugated rods", *International Communications in Heat and Mass Transfer*, Vol. 149, p. 107136.

Nishimura, T., Shiraishi, M., Nagasawa, F. and Kawamura, Y. (1988), "Natural convection heat transfer in enclosures with multiple vertical partitions", *International Journal of Heat and Mass Transfer*, Vol. 31 No. 8, pp. 1679-1686.

Paroncini, M., Corvaro, F., Montucchiari, A. and Nardini, G. (2012), "A numerical and experimental analysis on natural convective heat transfer in a square enclosure with partially active side walls", *Experimental Thermal and Fluid Science*, Vol. 36, pp. 118-125.

Raisi, A. and Arvin, I. (2018), "A numerical study of the effect of fluid-structure interaction on transient natural convection in an air-filled square cavity", *International Journal of Thermal Sciences*, Vol. 128, pp. 1-14.

Reddy, J. (1993), *An Introduction to the Finite Element Method*, Vol. 2, McGraw-Hill, New York, NY.

Sabeur-Bendehina, B.A.S., Adjlout, L. and Imine, O. (2006), "Effect of sinusoidal distribution of the temperature on laminar natural convection in wavy rectangular enclosures", *Journal of Applied Sciences*, Vol. 6 No. 3, pp. 710-715.

Saidi, C., Legay-Desesquelles, F. and Prunet-Foch, B. (1987), "Laminar flow past a sinusoidal cavity", *International Journal of Heat and Mass Transfer*, Vol. 30 No. 4, pp. 649-661.

Salehpour, A., Sadatlu, M. and Sojoudi, A. (2019), "Unsteady natural convection in a differentially heated rectangular enclosure possessing sinusoidal corrugated side walls loaded with power law non-Newtonian fluid", *Fluid Dynamics*, Vol. 54 No. 2, pp. 159-176.

Selimefendigil, F., Oztop, H. and Abu-Hamdeh, N. (2019b), "Impacts of conductive inner L-shaped obstacle and elastic bottom wall on MHD forced convection of a nanofluid in vented cavity", *Journal of Thermal Analysis and Calorimetry*, Vol. 141 No. 1, pp. 1-18.

Selimefendigil, F. and Oztop, H. (2016), "Analysis of MHD mixed convection in a flexible walled and nanofluids filled lid-driven cavity with volumetric heat generation", *International Journal of Mechanical Sciences*, Vol. 118, pp. 113-124.

Selimefendigil, F. and Oztop, H. (2019), "MHD mixed convection of nanofluid in a flexible walled inclined lid-driven L-shaped cavity under the effect of internal heat generation", *Physica A: Statistical Mechanics and Its Applications*, Vol. 534, pp. 122-144.

Selimefendigil, F. and Oztop, H. (2017), "Mixed convection in a partially heated triangular cavity filled with nanofluid having a partially flexible wall and internal heat generation", *Journal of the Taiwan Institute of Chemical Engineers*, Vol. 70, pp. 168-178.

Selimefendigil, F., Oztop, H. and Chamkha, A. (2019a), "MHD mixed convection in a nanofluid filled vertical lid-driven cavity having a flexible fin attached to its upper wall", *Journal of Thermal Analysis and Calorimetry*, Vol. 135 No. 1, pp. 325-340.

Selimefendigil, F., Oztopztop, H. and Chamkha, A. (2017), "Fluid-structure-magnetic field interaction in a nanofluid filled lid-driven cavity with flexible side wall", *European Journal of Mechanics - B/Fluids*, Vol. 61, pp. 77-85.

Shahabadi, M., Mehryan, S.A.M., Ghalambaz, M. and Ismael, M. (2021), "Controlling the natural convection of a non-Newtonian fluid using a flexible fin", *Applied Mathematical Modelling*, Vol. 92, pp. 669-686.

Shandar, K., Panda, S. and Reddy, E.S. (2025), "Natural convection of newtonian nanofluid with temperature-dependent viscosity in a wavy trapezoidal cavity: a numerical study", *The European Physical Journal Special Topics*, pp. 1-24.

Sheikholeslami, M., Gorji-Bandpy, M., Ganji, D. and Soleimani, S. (2014), "Natural convection heat transfer in a cavity with sinusoidal wall filled with CuO-water nanofluid in presence of magnetic field", *Journal of the Taiwan Institute of Chemical Engineers*, Vol. 45 No. 1, pp. 40-49.

Sheremet, M., Pop, I. and Roşca, N. (2016), "Magnetic field effect on the unsteady natural convection in a wavy-walled cavity filled with a nanofluid: Buongiorno's mathematical model", *Journal of the Taiwan Institute of Chemical Engineers*, Vol. 61, pp. 211-222.

Tekkalmaz, M. (2013), "Natural convection heat transfer and air flow in rectangular enclosures with a wavy wall", *Journal of Thermal Science and Technology*, Vol. 33 No. 1, pp. 21-31.

Wang, S. and Davidson, J. (2016), "Fluid-structure interaction in the flexible porous stratification manifold", *Journal of Solar Energy Engineering*, Vol. 138 No. 1, p. 11005.

Yaseen, D.T., Salih, S.M. and Ismael, M.A. (2023), "Effect of the lid-driven on mixed convection in an open flexible wall cavity with a partially heated bottom wall", *International Journal of Thermal Sciences*, Vol. 188, p. 108213.

**Corresponding author**
Ammar I. Alsabery can be contacted at: ammar_e_2011@yahoo.com